PERGAMON

International Journal of Heat and Mass Transfer 41 (1998) 3705–3718

International Journal of HEAT and MASS TRANSFER

Heat and mass transfer from internal flows to hemispheres and flat parts in between

F. L. A. Ganzevles, C. W. M. van der Geld*

Eindhoven University of Technology, Faculty of Mechanical Engineering, P.O. Box 513, 5600 MB Eindhoven, The Netherlands

Received 2 December 1997; in final form 6 March 1998

Abstract

With the naphthalene sublimation technique, the mass transfer from hemispheres on a flat plate to air flowing between two parallel plates is measured. A length scale is introduced to render the correlation of the results independent of the drop size. Measured mass transfer from flat plates is compared to measured heat transfer to flat plates. With the aid of the findings, mean interface temperatures of condensate drops in a compact PVDF heat exchanger are predicted. The calculations are compared with temperatures measured with an infrared camera.

Nomenclature

A surface [m^2]
c molar fraction
c_p heat capacity at constant pressure [J kg^{-1} K^{-1}]
d_1 length coolant channel in direction of the gas flow [m]
d_2 length coolant channel perpendicular to the gas flow direction [m]
d_3 thickness of the condenser wall between gas and coolant [m]
d_4 distance between gas side surface and center of coolant channel [m]
d_{drop} diameter hemispherical droplet [m]
D_H hydraulic diameter
$\mathbb{D}$ diffusion coefficient [m^2 s^{-1}]
h heat transfer coefficient [W m^{-2} K^{-1}]
$\tilde{h}$ enthalpy [J kg^{-1}]
h_m mass transfer coefficient [m s^{-1}]
H distance between two condenser plates [m]
L length of the heat exchanger plate in coolant direction [m]
L_{eff} effective length controlling gas boundary layer thickness, see equation (14) [m]
$\dot{m}$ mass flow rate [kg s^{-1}]
M molar mass [kmol kg^{-1}]
$\dot{M}$ mass flux [kg m^{-2} s^{-1}]
Q heat flow rate [W]
p pressure [Pa]
s distance between two successive channels [m]
T absolute temperature [K]
u velocity [m s^{-1}]
W length of heat exchanger plate in gas flow direction [m]
x coordinate in gas flow direction [m]
y coordinate perpendicular to the gas flow direction [m].

Greek symbols

α_{or} discharge coefficient
ε expansion coefficient
ζ length unit cell divided by d_{drop}, see Fig. 11
η dynamic viscosity [Pa s]
λ thermal conductivity [W m^{-1} K^{-1}]
ξ wetted area fraction
ρ mass density [kg m^{-3}]
σ surface tension [N m^{-1}]
φ relative humidity
χ_{conf} configuration factor
ω mass fraction (kg kg^{-1} mixture).

Subscripts

b bulk
cond condensate
cool coolant

* Corresponding author. E-mail: c.w.m.v.d.geld@wtb.tue.nl

0017–9310/98 $19.00
PII: S0017–9310(98)00117–3

g gas
in inlet
int interface
liq liquid
L_{eff} based on L_{eff} rather than D_H
na naphthalene
out outlet
pl plate, condenser wall
sat saturated
tot total
vap water vapor
w wall.

Acronyms
Nu Nusselt number, $h \cdot D_H/\lambda$
Pr Prandtl, $\eta \cdot c_p/\lambda$
Re Reynolds number, $\rho \cdot v \cdot D_H/\eta$
Se Schmidt number, $\eta/(\rho \cdot \mathbb{D})$
Sh Sherwood number, $h_m \cdot D_H/\mathbb{D}$.

1. Introduction

The exhaust gases of e.g. power plants contain a large amount of recoverable energy. When this energy is recovered, the gas temperature lowers in the stack, possibly to the acid dew point of the exhaust gases (SO_x). If the dew point is reached, corrosion and erosion usually occur but, at the same time, the energy release becomes favorably high by the release of condensation enthalpy. Especially if dropwise condensation occurs, rather than filmwise, the energy exchange is very effective [1].

The rate of condensation depends, amongst other things, on:

- the interface temperature,
- the Sherwood number of the geometry at hand.

In dropwise condensation, usually little is known about these parameters. The presence of inert gases causes the interface temperature to vary at the surface of a drop and reduces the Sherwood number as well as heat transfer [2–4]. The geometry obviously is an important governing parameter. In any prediction method of the rate of condensation and the interface temperature, the influence of the geometry has to be accounted for, e.g. by using the appropriate Sherwood and Nusselt numbers.

In this paper, mass transfer is directly measured in geometries that are relevant for dropwise condensation in compact heat exchangers. The naphthalene sublimation technique is applied. This technique was used by, for example, Hu et al. [5] for droplets on finned tubes, by Goldstein et al. [6] for pin-fins and Payvar et al. [7] for grooves. An alternative method would have been the electrochemical method of an aqueous solution of ferricyanide complex ions [8]. However, this method requires a delicate tuning (in darkness) and the scaling of liquid–solid to gas–liquid mass transfer.

The principal geometry studied in this paper is that of hemispheres on flat plates, for which no data have been found in the literature. In dropwise condensation of air–steam mixtures on plastic condenser plates, the condensate drops are hemispherical since the contact angle between PVDF (PolyVinyliDeneFluoride) and water is ca 90°. The condenser plates are covered with droplets with a maximum radius of 1.65 mm at a wetted area fraction of around 36% [9]. The results of the napthalene technique will be validated with the transfer coefficients measured for heat transfer to flat plates. For the generalization of the experimental findings, it is investigated what length scales are relevant, and how they can be accounted for.

The results are directly applicable in a method to predict the mean interface temperature of condensate drops [10]. Predictions with the new correlations will be compared with in situ temperature measurements, with an infrared camera, during condensation of air–steam in a compact, plastic heat exchanger.

2. Experimental

2.1. *Test rig*

A compact PVDF (PolyVinyliDeneFluoride) plate heat exchanger is mounted in a wind tunnel with an inlet length of 12 m. Ambient air is blown through a duct, 200 mm in diameter, in which, according to DIN 1952 [11], an orifice, ∅ 150 mm, is mounted (see Fig. 1). The pressure drop over the orifice is measured with an inclined tube-manometer with an accuracy of 0.1% of full scale (1 kPa). The inlet gas mass flow rate, $\dot{m}_{g,in}$, is determined with an accuracy better than 1%. Before the gas flow passes the orifice the air is heated via two heat exchangers, capacities 40 and 80 kW. A steam generator produces dry steam at 182°C and 1 MPa, with a maximum capacity of 957 kW. The steam pressure is reduced to a constant value of 0.78 MPa to prevent pressure and temperature fluctuations. Remaining fluctuations are analyzed in Section 3.1. Part of the steam can be injected into the air, see Fig. 1. In this paper, this is only done for the measurements to be described in Section 2.4. The gas mixture enters two identical compartments, see Fig. 2. The velocity profiles have been measured in each compartment just up and downstream of the heat exchanger with a Prandtl tube. In both compartments the flow is laminar and the mass flow rates are equal. The inlet and outlet temperatures of each compartment, $T_{g,in}$ and $T_{g,out}$, respectively, are measured at four locations with calibrated multiple electrical resistance thermometers, type PT 100 class A according to DIN IEC 751, with an accuracy of 0.1°C. The inlet and outlet temperatures are averaged over the height, weighed by the corresponding mass velocity.

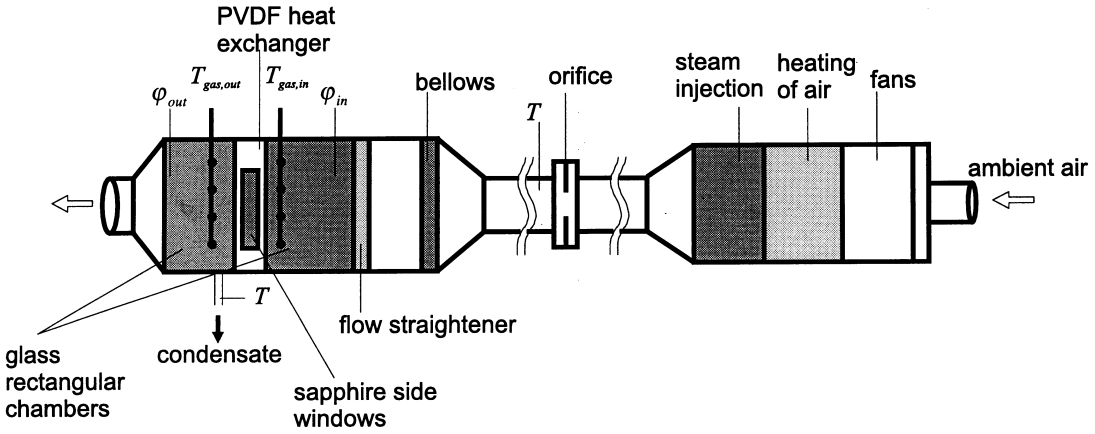

Fig. 1. Schematic of the test rig. Only one of the two separate measuring compartments is shown.

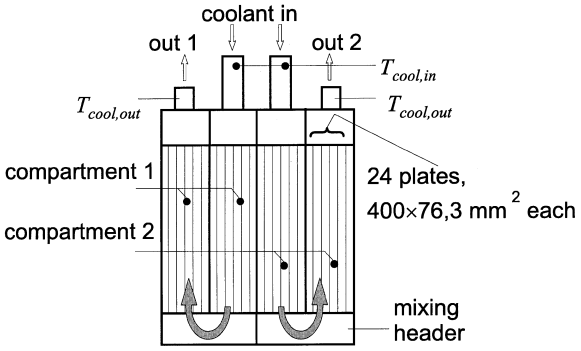

Fig. 2. Front view of heat exchanger, test unit.

The inlet and outlet relative humidities, φ_{in} and φ_{out}, are measured with calibrated Vaisala HMP-135Y sensors, accuracy better than 1%. The vapor mass concentration in an air–steam mixture, ω_{vap}, follows from the well-known equation

$$\omega_{vap} = \varphi \cdot p_{sat} \Big/ \left(\varphi \cdot p_{sat} + \frac{M_{air}}{M_{vap}} (p_{air} - \varphi \cdot p_{sat}) \right) \quad (1)$$

with the molar mass of dry air given by M_{air}, and that of vapor by M_{vap}. The saturation pressure, p_{sat}, is determined from the Antoine relation for water vapor [12]. Most measurements in this paper are without condensation. In that case, the vapor mass concentration measured at the outlet has a higher accuracy than that at the inlet because of the lower temperature.

Each of the four sections of the exchanger encompasses 24 parallel plates, separated by 2.0 mm with a length (height), L, of 400 mm, a width W of 76.3 mm and a thickness of 2.0 mm, see Fig. 2. In each plate there are 42 ducts, see Fig. 3, with dimension of $d_1 \times d_2$, 1.37 mm × 1.47 mm. The thickness $d_3 = 0.27$ mm. The conductive heat resistance of the plate depends on s and d_1, in a way described in an earlier paper [13]. The coolant is water. The coolant temperatures, $T_{cool,in}$ and $T_{cool,out}$, are measured for each compartment at the inlet and outlet of the heat exchanger with PT 100's, accuracy 0.1°C. The coolant mass flow rate, $\dot{m}_{cool}$, is measured with Fischer & Porter FP-1-35 G 10/80 (stainless steel flat 1-GNSVT-66) flow meters for each compartment individually with an accuracy better than 1% of full scale (0.77 kg s^{-1}).

The entire test rig is heated during more than five quarters of an hour prior to the actual measurements. The remaining inlet coolant temperature variation is less than 0.05°C, as controlled by a PI device. The heat losses to the surroundings have been measured directly with two heat flux sensors, inaccuracy 1 W m^{-2}, with fluctuations due to draft, etc. 5 W m^{-2} typically.

The condensate is collected downstream of the heat exchanger in Erlenmeyer flasks via valves. The condensate temperature for each compartment is measured with fully wetted PT 100's, accuracy 0.1°C. Time and weight of collected condensate are measured to yield the condensate mass flow rate, $\dot{m}_{cool}$, directly.

The wetted area ratio and the temperature field at the two condenser sides are measured, through glass and sapphire windows, respectively. The attenuation depth of infrared light in the wavelength range used, 2–5.6 μm, is for water negligible in comparison with the droplet size, so drop interface and plate temperatures are measured. The measurement is contactless with an infrared camera, model thermovision system 680 (AGA infrared system). The temperature range is adjustable and the temperature offset arbitrary. The accuracy depends on the temperature range; in our case the accuracy is better than 0.2°C. The signal from the cooled detector, InSb in liquid nitrogen, is digitized and stored on hard disk at a rate of 0.16 frames s^{-1}. Each image, 120 × 128 points, has actual dimensions 50 × 50 mm^2, which is 610 pixels per cm^2. This gives each point a width of 0.4 mm.

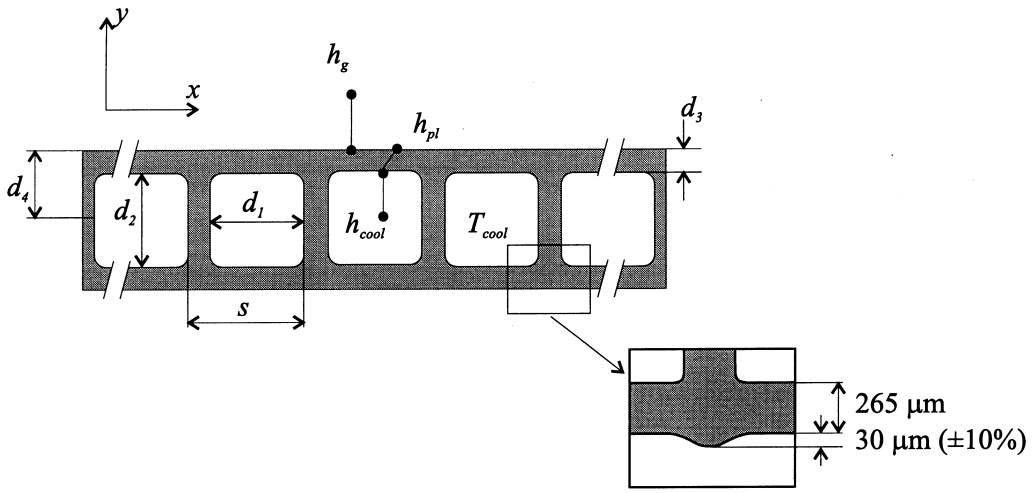

Fig. 3. Schematic cross-section of coolant channels in a PVDF condenser plate with view on surface indentation.

2.2. Determination of the gas-sided heat transfer coefficient

The heat flow rate to the coolant, in W, follows from

$$Q_{\text{cool}} = \dot{m}_{\text{cool}} \cdot (c_{\text{p}}(T_{\text{cool,out}}) \cdot T_{\text{cool,out}} - c_{\text{p}}(T_{\text{cool,in}}) \cdot T_{\text{cool,in}}) \tag{2}$$

with $\dot{m}_{\text{cool}}$ the coolant mass flow rate, in kg s^{-1}. In equation (2) c_{p} is the specific heat at constant pressure and T the absolute temperature. The temperatures in relation (2) are all measured.

In a cross-flow heat exchanger the heat flow rate from gas to coolant can also be written [14] as

$$Q_{\text{cool}} = h_{\text{tot}} \cdot A_{\text{g}} \cdot \chi_{\text{conf}} \cdot (\Delta T_{\text{a}} - \Delta T_{\text{b}}) / \ln(\Delta T_{\text{a}} / \Delta T_{\text{b}}) \tag{3}$$

with h_{tot} the total heat transfer coefficient, A_{g} the heat-exchanging surface at the gas-side, χ_{conf} a configuration factor, $\Delta T_{\text{a}} = T_{\text{g,in}} - T_{\text{cool,out}}$, $\Delta T_{\text{b}} = T_{\text{g,out}} - T_{\text{cool,in}}$. The factor χ_{conf} is typically 0.99 in our case [14].

The total heat transfer coefficient encompasses contributions from the coolant to the plate, h_{cool}, the one through the plate, h_{pl}, see Fig. 3, and that from the gas to the plate, h_{g}:

$$\frac{1}{A_{\text{g}} \cdot h_{\text{tot}}} = \frac{1}{A_{\text{cool}} \cdot h_{\text{cool}}} + \frac{1}{A_{\text{pl}} \cdot h_{\text{pl}}} + \frac{1}{A_{\text{g}} \cdot h_{\text{g}}} \tag{4}$$

where A_{cool} is the heat exchanging surfaces of the coolant-side. The heat transfer coefficient to the coolant, h_{cool} downstream of the entry region is 1530 (W m^{-2} K^{-1}), corresponding to $Nu_{\text{cool}} = 2.996$ [15]. In an earlier paper [13] we showed that the heat resistance of the condenser plate is given by

$$1 \Big/ (A_{\text{pl}} \cdot h_{\text{pl}}) = \frac{d_4}{s} \cdot 0.67 \cdot \pi \Big/ \ln\left(\frac{s}{0.728\pi \cdot r} \sinh\left(\frac{\pi \cdot d_4}{s} \right) \right) \tag{5}$$

with d_4 the distance between gas-side surface and centre coolant channel, s the distance between two successive coolant channels and $r = d_1^{0.14} \cdot d_2^{0.86}$ the effective radius of a coolant channel, see Fig. 3. The heat transfer coefficient of the plate is typically 540 W (m^{-2} K^{-1}) for the geometry of Fig. 3. The gas-sided heat transfer coefficient, h_{g}, is determined by substituting equations (4) and (5) in equation (3) and eliminating Q_{cool} from equations (2) and (3).

The heat flow rate to the coolant is alternatively given by the enthalpy balance at the gas side:

$$Q_{\text{cool}} = \dot{m}_{\text{g,in}} \cdot \tilde{h}_{\text{g}}(T_{\text{g}}, \omega_{\text{vap}})_{\text{in}} - (\dot{m}_{\text{g,in}} - \dot{m}_{\text{cond}}) \cdot \tilde{h}_{\text{g}}(T_{\text{g}}, \omega_{\text{vap}})_{\text{out}} - \dot{m}_{\text{cond}} \cdot \tilde{h}_{\text{cond}}(T_{\text{cond}}). \tag{6}$$

Here $\tilde{h}$ denotes the enthalpy and ω_{vap} the water vapor mass fraction in kg kg^{-1} mixture. The RHS of equation (6) contains only measured quantities. Comparisons will be made in Section 3.1.

2.3. Naphthalene measurements

Mass transfer measurements have been performed with the naphthalene[1] sublimation technique. It allows for the direct measurement of local mass transfer coefficients [5–7]. The results are generalized with the aid of the Schmidt number, $Sc = \eta_{\text{g}}/(\rho_{\text{g}} \cdot \mathbb{D}_{\text{na}})$, and the Sherwood number:

$$Sh = h_{\text{m}} \cdot D_{\text{H}} / \mathbb{D}_{\text{na}} \tag{7}$$

[1] $C_{10}H_8$, with molar mass 128.17 kg mol^{-1}, melting point 80–82°C, boiling point 218°C and solid mass density 997 kg m^{-3}.

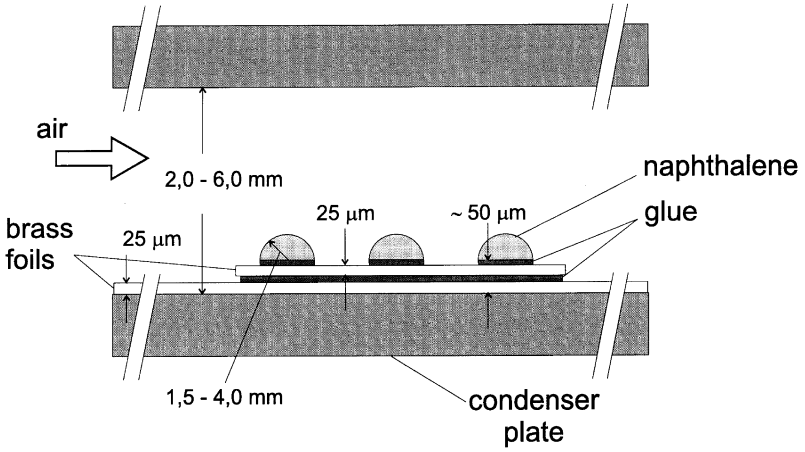

Fig. 4. Schematic of naphthalene hemisphere distribution on condenser plate. Drop centers are on an equidistant rectangular grid at rows parallel to the flow.

with h_m the mass transfer coefficient[2] in [m s^{-1}]. Here D_H is the hydraulic diameter, defined as four times the cross section area divided by the perimeter. In our case $D_H = 4 \cdot H \cdot L/(2 \cdot H + 2 \cdot L)$, which equals[3] 3.98 mm. The diffusion coefficient of naphthalene, $\mathbb{D}_{na}$ is sensitive to temperature variation. A typical value for naphthalene in air is $6.38 \cdot 10^{-6}$ m^2 s^{-1} at 20°C [17, 18]. A relation valid for temperatures in 287.67–327.11 K is given by Cho et al. [18]:

$$\mathbb{D}_{na} = 8.17708 \cdot 10^{-7} T^{1.983}. \quad (8)$$

Cho et al. [18] also give a correlation for the Schmidt number of naphthalene: $Sc = 8.0743 \cdot T^{-0.2165}$. The following three naphthalene configuration samples are placed in the PVDF exchanger, each in a different channel:

(i) a flat surface,
(ii) hemispherical droplets on a equidistant rectangular grid with flow parallel to the rows of drops (see Fig. 4),
(iii) a flat surface with hemispherical droplets on the same grid as (ii).

All three configurations are simultaneously measured to improve the accuracy of the comparison by avoiding temperature correction, see equation (8). The distance between neighboring condenser plates, H, is varied in 2.0–6.0 mm, see Fig. 4. The inlet velocity of each channel is measured with Prandtl tubes.

The hemispheres are manufactured by letting molten naphthalene (85°C) fill up a mould of greasy, dehumified clay. Twelve drops with a diameter of 3–8 mm are glued on a brass foil, 20×30 mm^2 and a thickness of 0.025 mm, which is glued on a larger brass foil, 75×50 mm^2 and a thickness of 0.025 mm, see Fig. 4. Sublimation and evaporation of the glue, measured during a 4 h test run, is less than 0.1 mg, which is negligible. The distance between drops has been selected such, that the ratio of projected drop surface area to total area, ξ, is 0.33. This ratio corresponds to the wetted area fraction during actual condensation on PVDF [9]. This is further discussed in Section 3.4. During $\Delta t = 3600$ s ($H = 2$ mm) or 1800 s ($H = 6$ mm) air isothermally flows over the napthalene. The time span Δt has been chosen such that the decrease of the mass transfer area of naphthalene surface in contact with the gas, A_{na}, is negligible, which depends on the drop size and the inlet Reynolds value. The weight loss, Δm, is measured with a Mettler AE200 precision scale (± 0.1 mg).

The mass transfer coefficient, h_m, is determined from the measured quantities as

$$h_m = \frac{\Delta m}{A_{na} \cdot \Delta t \cdot \rho_{na}}. \quad (9)$$

Here ρ_{na} is the saturation mass density of the vapor phase, determined from the ideal gas law $\rho_{na} = p_{na,sat}/(R_{na} \cdot T)$. The saturation pressure, $p_{na,sat}$, is tabulated by Ambrose et al. [17].

[2] Bird et al. [16] utilize $k_x/\tilde{c} = h_m$ with $\tilde{c}$ the molar concentration in [mol m^{-3}] and k_x the molar mass transfer coefficient in [mol (s^{-1} m^{-2})].

[3] The gap between two successive plates is 2.00 mm and the length of the plate in coolant direction is 400 mm.

2.4. Prediction of the average interface temperature

A way to predict the mean condensate interface temperature from the measured steam concentration in the bulk, $\omega_{vap,b}$, in kg kg^{-1} mixture, was given by van der Geld and Brouwers [10]. This method requires the measurement of the condensate mass flux, $\dot{M}_{cond}$, and uses

$$\dot{M}_{cond} = -\rho_g \cdot h_{m,vap} \cdot \ln\left(\frac{1-\omega_{vap,b}}{1-\omega_{vap,int}}\right) \quad (10)$$

with ρ_g the mass density of the gas mixture and $h_{m,vap}$ the mass transfer coefficient of water vapor known from a correlation. Equation (10) yields the saturated water vapor concentration, $\omega_{vap,int}$, that is related to the saturation temperature of the drop interface via the Antoine relation [12] and equation (1) with $\varphi = 1$. This average interface temperature is the result desired.

The method will be applied in Section 3.6.

3. Results and analysis

3.1. Convective heat transfer coefficients

In the measurements of this section, the gas Reynolds number of the channel, $Re_{D_H} = \rho_g \cdot u \cdot D_H/\eta_g$, has been varied in 600–1400, which correspond to mass flow rates of 0.13–0.28 kg s^{-1} per compartment. The inlet gas temperature, $T_{g,in}$, has been varied in 70–97°C and the water vapor pressure at the inlet was 1 kPa or less, making φ_{in} as low as 0.6–2.3%. The inlet coolant temperature, $T_{cool,in}$, has been kept constant at a temperature of 24.95 ± 0.05°C except for six runs when the coolant inlet temperature is 19.87 ± 0.07°C. A total of 53 runs have been performed: 20 with a coolant mass flow rate, $\dot{m}_{cool}$, of 0.3 ± 0.007 kg s^{-1} and 33 with $\dot{m}_{cool} = 0.6 \pm 0.007$ kg s^{-1}.

The accuracy of the measurements is exhibited in the results of Figs 5 and 6. Figure 5 shows typical time traces of gas and coolant temperatures for $\varphi_{in} = 1.9\%$, $Re_{g,in} = 970$ and $\dot{m}_{cool} = 0.6$ kg s^{-1} ($Re_{cool,in} = 430$). The influence of the low frequency drift of $T_{g,in}$ and $T_{cool,in}$, has been minimized by computing temperature differences, ΔT, in coolant and gas before averaging. In the first time interval of 10 min in Fig. 5, the maximum ΔT-variation is 0.12 K top–top.

Figure 6 shows a comparison of the two heat flow rates that have been measured independently: Q_{cool} and Q_{gas}, see equations (2) and (6). The heat losses through the thermal isolation have been measured to be negligible, namely 20 ± 4 W m^{-2} and 10 ± 2 W between inlet and outlet measuring points of the two compartments. Q_g and Q_{cool} are therefore found to be the same. The deter-

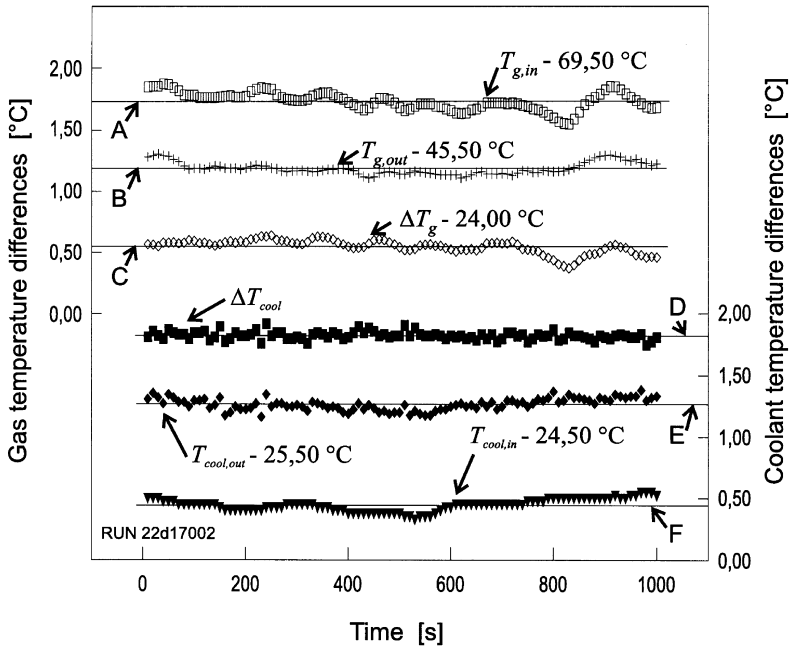

Fig. 5. Typical histories of coolant and gas temperatures at the inlet and outlet. The $T_{gas,in}$-curve is shifted by 69.50°C for sake of convenience. Inlet conditions are: $Re_{g,in} = 970$, $\varphi_{in} = 1.9\%$ and $\dot{m}_{cool} = 0.300$ kg s^{-1} ($Re_{cool} = 418$). The weighed average over 100 data during 1000 s and the corresponding standard deviation (RMS), as indicated with solid lines, are: A: $\bar{T}_{gas,in} = 71.23 \pm 0.07$°C; B: $\bar{T}_{gas,out} = 46.69 \pm 0.05$°C; C: $\Delta\bar{T}_{gas} = 25.55 \pm 0.06$°C; D: $\Delta\bar{T}_{cool} = 1.83 \pm 0.03$°C; E: $\bar{T}_{cool,out} = 26.77 \pm 0.05$°C and F: $\bar{T}_{cool,in} = 24.95 \pm 0.05$°C.

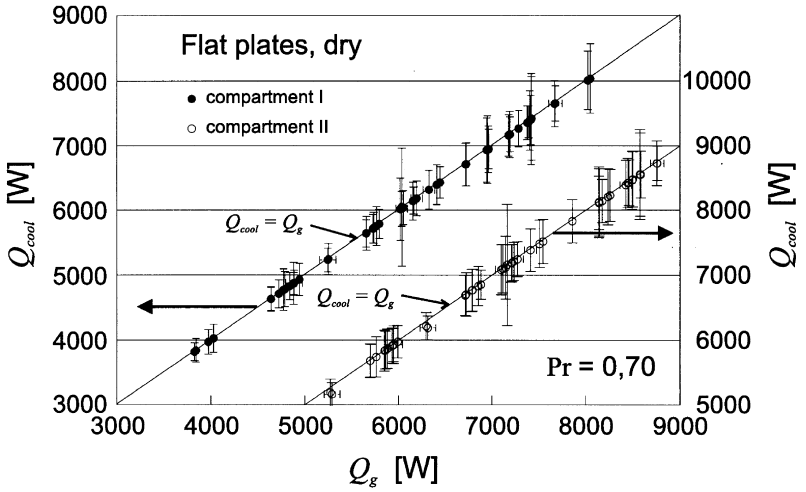

Fig. 6. Comparison of heat flow rates Q_g and Q_{cool}, measured independently during 53 tests in both compartments.

mination of the total heat flux between gas and coolant in the absence of condensation turns out to be more accurate with the measured gas parameters than with the coolant parameters. Note that the coolant temperature drop is typically 2–3°C (Fig. 5), whereas ΔT_g is typically 24°C. The main contribution to the error in Q_{cool} stems from the relative error in ΔT_{cool}, which is relatively large. The resulting total error in Q_g is less than 1% typically. The two compartments yield identical results, see Fig. 6.

The Nusselt number is defined $Nu = h_g \cdot D_H/\lambda_g$ in which λ_g is the thermal conduction coefficient of the gas. The measured Nu-values of both compartments in the absence of condensation, with φ_{in} in 0.6–2.3%, are given in Fig. 7. The two compartments yield identical results for both values of $\dot{m}_{cool}$. Nu is seen to depend on the coolant mass flux. The low $\dot{m}_{cool}$-values have been correlated according to

$$Nu = (6.8 \pm 0.2) + (0.0016 \pm 0.0002) \cdot Re \cdot Pr^{1/3} \quad (11)$$

and the high $\dot{m}_{cool}$ values according to

$$Nu = (6.9 \pm 0.1) + (0.0017 \pm 0.0002) \cdot Re \cdot Pr^{1/3}. \quad (12)$$

The given error is twice the standard deviation [19]. Equations (11) and (12) are valid for Re_{D_H} in 600–1400. The exponents of Re and Pr have been fixed. Lowering the exponent of Re from 1 to 0.7 improved the corrected r^2 value of the fit from 0.91 to 0.92. For the lower $\dot{m}_{cool}$-values Nu is lower. This case corresponds to more inhomogeneous coolant temperatures. At higher coolant mass flow rates the temperatures of both coolant and exchanger plate are obviously more uniform. The low $\dot{m}_{cool}$-case corresponds better to the case of heat transfer with condensation since temperature differences on the plate are larger if the heat flux to the plate is.

The dependency of Nu on Re, as given by the data of Fig. 7, is more pronounced as that given by Stephan [20]. The latter theoretical dependency merely accounts for the entrance effect:

$$Nu = a + b \cdot \frac{(Re \cdot Pr \cdot D_H/W)^{1.14}}{1 + 0.0358 \cdot (Re \cdot Pr \cdot D_H/W)^{0.64} \cdot Pr^{0.17}} = a + b \cdot f(Re, Pr, D_H/W) \quad (13)$$

$a = 7.55$ for isothermal walls and $a = 8.23$ for constant heat flux at the walls. In both cases b is 0.024. Equation (13) defines f, introduced for ease of reference in later figures; values of f are indicated on the top of Figs 7 and 8. Equation (13) was derived for two infinitely large, parallel plane walls. Shah and London [15] also applied relation (13) to a finite extend of the plates. If the short sides are adiabatic, they derived $a = 7.27$ (uniform temperature) and 7.95 (uniform heat flux).

Equation (13) predicts a gradual increase of Nu with increasing Re ($\Delta Nu/\Delta Re = 9.6 \cdot 10^{-4}$) whereas the data show a dependency that is approximately twice as large ($\Delta Nu/\Delta Re \approx 1.6 \cdot 10^{-3}$). It is concluded that the Reynolds dependency measured is not primarily due to the entrance effect. It is possibly caused by the slight indentations of the plates, making them not perfectly flat, but varying by 0.1 per 1.87 mm, see Fig. 3. The indentations are due to the fabrication process (extrusion).

The analogy of heat and mass transfer [16] makes it possible to derive correlations for mass transfer from correlations for the Nusselt number, by replacing the Prandtl number $Pr = \eta_g \cdot c_{p,g}/\lambda_g$ by $Sc = \eta_g/(\rho_g \cdot \mathbb{D}_{vap})$. Nusselt values for 'dry' experiments in this way yield Sherwood numbers, see equation (7), for flat plates. Resulting Sherwood numbers will be compared with the directly measured ones of the following section.

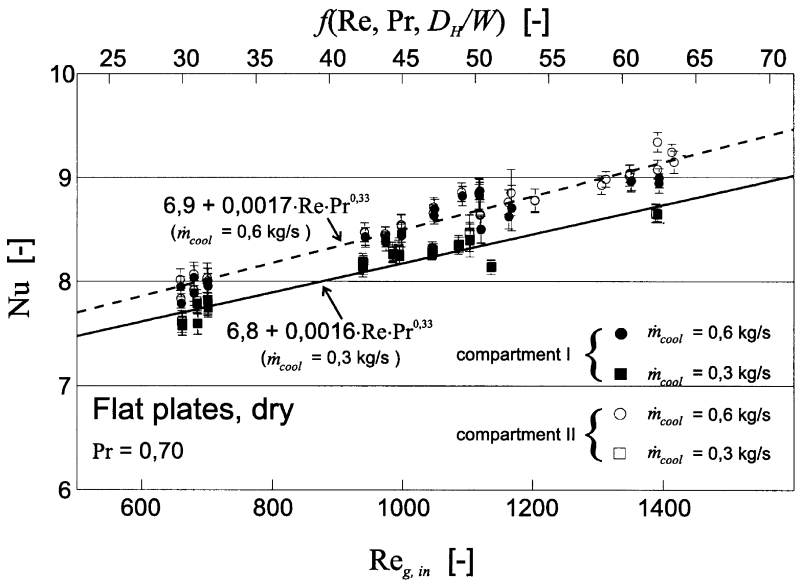

Fig. 7. Nusselt numbers measured without condensation, 'dry', in both compartments; $T_{cool,in} = 25°C$. Because of the large heat flux with condensation the $\dot{m}_{cool} = 0.3$ kg s^{-1} case mimics the temperature and *Nu*-variation of condensation best. The $\dot{m}_{cool} = 0.6$ kg s^{-1} case mimics the isothermal case, see Fig. 8.

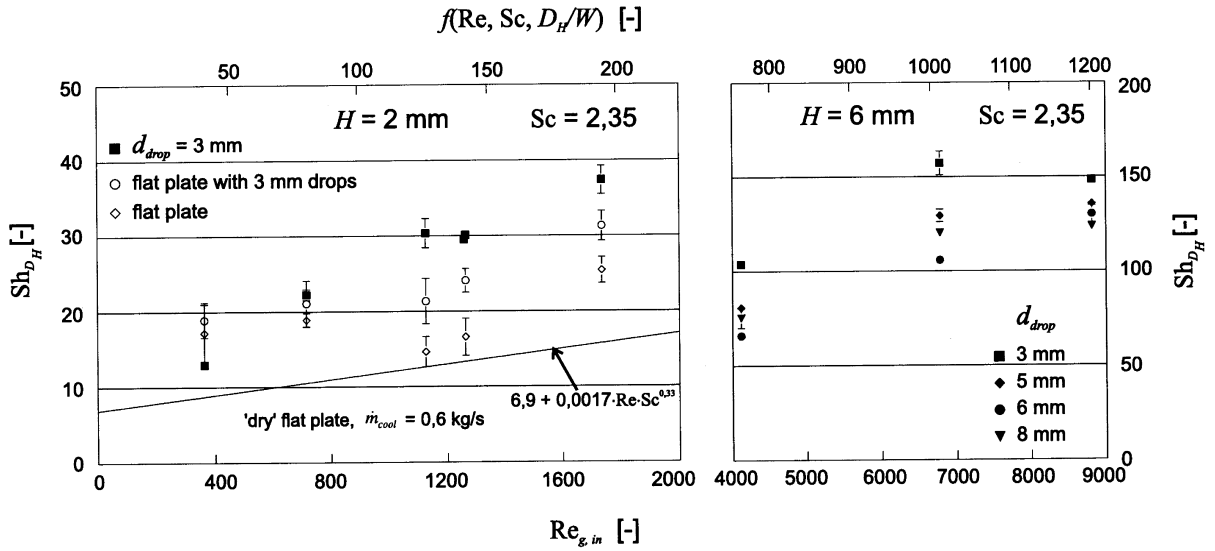

Fig. 8. Sherwood numbers, based on $D_H = 4$ mm and $D_H = 12$ mm, measured with the naphthalene sublimation technique. Compartment II, adapted for $H = 6$ mm case. Inlet gas velocity measured with Prandtl tube.

3.2. Convective mass transfer coefficients

Measured values of the mass transfer coefficient, h_m, see equation (9) are expressed in terms of the Sherwood number, *Sh*, see equation (7). Results of naphthalene experiments with the three geometries described in Section 2.3 are gathered in Fig. 8 in terms of Sh_{D_H}, in which the characteristic length L is taken to be the hydraulic diameter. For $Re_{g,in} < 2000$, the measurement results are for hemispheres only (filled squares), for flat plates without hemispheres (open diamonds) and for the combination of flat plate parts with hemispheres (open circles). The arrangement of hemispheres is rectangular as described in Section 2.3. The accuracy of Sh_{D_H} is ca

3%. It is clearly seen that the Sherwood number of hemispheres exceeds that of flat parts, by approximately 100%. This has to be accounted for in the method to compute the average interface temperature, see Section 2.4. The correlation (12) found above for the Nusselt number of convective heat transfer has been used to compute *Sh*-numbers by replacing *Pr* by the appropriate Schmidt number, $Sc = 2.35$ [18]. The result is shown in Fig. 8 as a straight line. The correlation (12) has been used rather than (11) since the process of naphthalene sublimation is isothermal. The naphthalene results for flat plates only (open diamonds) have a tendency to exceed the correlation (12). This tendency might be caused by the residual temperature inhomogeneity of the plates in the measurements on which the correlation is based. Values of Nu for the fully isothermal case are theoretically lower than that of other cases, see [15].

Sherwood numbers for flat parts in between drops are expected to be lower than that of drops only because of the lower values for flat plates only, see above, and because of the wakes of the drops. Horseshoe vortices probably occur at the downstream side of drops in which mixing is low. Heat transfer augmentation may only be expected if the vortices are periodically shed from the drops [21]. The wakes will be further investigated in Section 3.3. The *Sh*-values for the combination of plate and drops in Fig. 8 lie indeed in between those of drops only and plate only.

For $Re_{g,in} > 4000$, the ratio d_{drop}/H is in Fig. 8 seen to affect mass transfer from drops only. The smaller drops have the higher mass flow rate. In the computation of interfacial temperatures, see Section 2.4, the use of a mass transfer coefficient that depends on d_{drop} would complicate the averaging of the mass transfer equation. In the following it is therefore attempted to interpret the above dependency of Sh_{D_H} on d_{drop} and to produce a unified correlation for the Sherwood number.

3.3. Numerical simulation

The interpretation of the mass transfer measurements is facilitated by some numerical modeling results. Figure 9 shows the part of the grid, used for a 2-D finite element computation, that is in the area around the drop. The inlet gas velocity and temperature, about $10 \cdot d_{drop}$ upstream, i.e. in the negative *x*-direction, are taken uniform: 5 m s^{-1} and 70°C, respectively. The bottom and top temperatures are that of the PVDF plate in contact with the coolant. They increase from 24–29°C over 76 mm, in the positive *x*-direction. At the drop surface, the no-slip boundary condition is applied because of the low viscosity ratio η_g/η_{liq}. The interface does not deform because of the low value of $We = \rho \cdot u^2 \cdot L/\sigma$, which is confirmed by observations of hemispherically shaped condensation drops. The condensation enthalpy freed at the droplet interface is given the value 5.99 W m^{-2}, based on our measurements of heat transfer, average drop size and number of drops [9]. The transient computations have been performed with FIDAP™, and typically required 46.2 s of process time on a Silicon Graphics Power Challenge (14 MIPS IP21, CPU MIPS R8000 64 bits 75 MHz revision 2.2 and RPU MIPS R8010 revision 0.1). The time step is 2 μs, the number of steps is 5000. Upstream of the drop, flow is internal since the boundary layers at the two plates have touched. This implies that the distance between the plates, H is a length scale of importance.

In the computation of Fig. 10, the boundary layer detaches at an angle of ca 120° from the upstream three-phase point (drop foot). An elliptic wake is established downstream. Velocities and temperatures are lower in the wake than in the outer flow region. In this transient computation, the wake is stagnant and extends several drop diameters, but in actual 3-D situations with drops at a row the wake volume is expected to be smaller and vortex shedding may occur. Near the top of the drop, the gas is accelerated and the boundary layer is thin, causing convective heat (and mass) transfer to be high. Near the top of the drop, where the distance between isotherms is smallest, heat transfer is highest and even a kind of stagnation point is observed. The ratio $(H-d_{drop})/H$ determines the acceleration and hence the heat transfer augmentation on the top of the drop. Also d_{drop} is therefore a length scale of importance.

Condensation enthalpy release is that large, as compared to convective heat transfer, that the interface temperature is symmetrical with respect to the line through the crest of the drop normal to the condenser plate. This conclusion also holds for actual condensation drops, as was validated with the aid of infrared recordings [22]. In the wake, mixing is poor and the quality of heat transfer strongly depends on the periodicity at which large-scale vortices are being shed [21]. This periodicity is unknown for the configuration of hemispheres in an array on a plate, that was measured in Section 3.2. However, the higher net convective mass transfer values for drops only, as compared with flat plate results in Fig. 8, are easily understood from the higher convective heat transfer at the upstream side of the drop, see Fig. 10, and the analogy of heat and mass transfer. However, the 2-D gas acceleration above the drop does not cause the dependence of *Sh* on d_{drop}, since with increasing drop diameter, Sh_{D_H} decreases (see Fig. 8) whereas the 2-D gas acceleration above the drop increases. The crucial factor here is the constant wetted area fraction, ξ, of the actual 3-D geometry. The frontal area per drop for the gas to pass through depends on the number of drops, and therefore, with constant ξ, on d_{drop}. In the experiments of Section 3.2, both ξ and the number of drops have been kept constant (0.33 and 12, respectively), resulting in a decreasing distance between drops with decreasing drop diameter. The frontal area available to each drop is

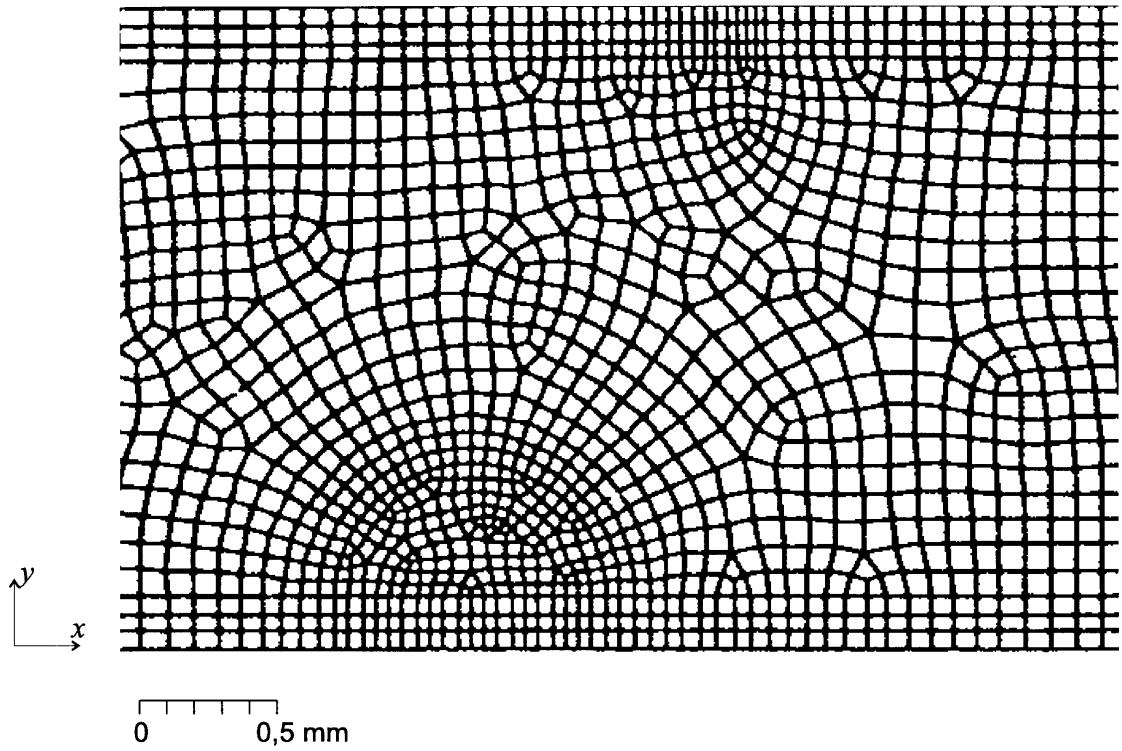

Fig. 9. Schematic plan-view of part of the composite grid use for computation.

schematized in Fig. 11, with ζ the inverse of the wetted area fraction. The available flow area per 'unit cell' increases with increasing d_{drop}, yielding a decreasing average velocity and hence lower mass transfer rates. This trend is also observed in Fig. 8 ($Re_{g,in} > 4000$).

In the next section, the unit cell is used to take the two length scales involved, d_{drop} and H, into simultaneous account.

3.4. In search of a representative characteristic length

Let L_{eff} be the hydraulic diameter of a unit cell (see Fig. 11):

$$L_{eff} = \frac{4\cdot(H\cdot\zeta\cdot d_{drop} - \pi\cdot d_{drop}^2)}{(\zeta-1)\cdot d_{drop} + \zeta\cdot d_{drop} + \pi\cdot d_{drop}/2 + 2\cdot H} \cong 2\cdot H \Big/ \left(1 + \frac{1}{\zeta}\cdot\frac{H}{d_{drop}}\right). \quad (14)$$

For the measurements of Section 3.2, d_{drop} is precisely known. For condensation measurements, the measured average drop diameter can be used. If both the Sherwood and Reynolds numbers are based on L_{eff}, the measuring points of Fig. 8 are shifted with respect to each other.

The value of ζ in equation (14) has been varied in order to decrease differences between naphthalene measurement results of various drop sizes. A good value for ζ turned out to be three. This value corresponds to an average wetted area fraction, ξ, of 33%, which is not only quite realistic [9], but also precisely the one used in the experiments here analyzed. In Fig. 12, both *Sh* and *Re* are based on L_{eff} with $\zeta = 3$. The corrected r^2-value of the linear fit through all the data is 0.955, whereas the r^2-value of a fit through the data of Fig. 8 is 0.877. This seems to indicate that the physical phenomena involved in mass transfer from hemispheres in between two flat plates are better captured by the length scale L_{eff} than by the hydraulic diameter, $2H$. The flow and mass transfer situation during condensation heat transfer being essentially more complex, the appropriate value of L_{eff} might, however, not only depend on the wetted area fraction, ξ (via ζ), but also on the value of d_{drop} selected. As suggested above, the average drop diameter is a good candidate, but since the gas flow pattern is strongly affected by the largest drops, some value closer to the maximum drop size could equally well be appropriate. This is beyond the scope of the present investigation. For the naphthalene measurements of Section 3.2, d_{drop} is unambiguously known, and ζ and L_{eff} well-defined. The unified correlation for $Sh_{L_{eff}}$ in this case is given by

$$Sh_{L_{eff}} = (13 \pm 5) + (0.010 \pm 0.001)\cdot Re_{g,in}\cdot Sc^{1/3}. \quad (15)$$

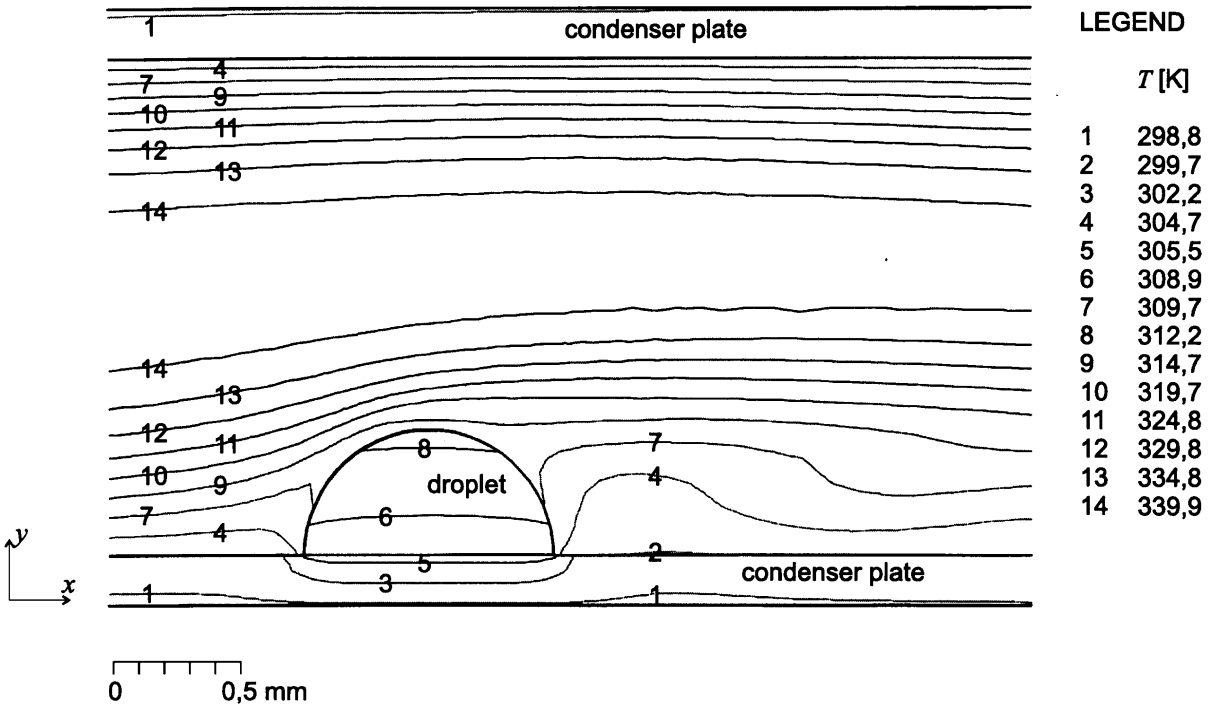

Fig. 10. Finite element transient computation of 2-D temperature profiles. Drop is static. The PVDF-plate has a bottom temperature linearly increasing in x-direction from 24–29°C. A uniform line heat source of 5.99 kW m^{-2} is situated at the entire drop surface to simulate the condensation enthalpy release.

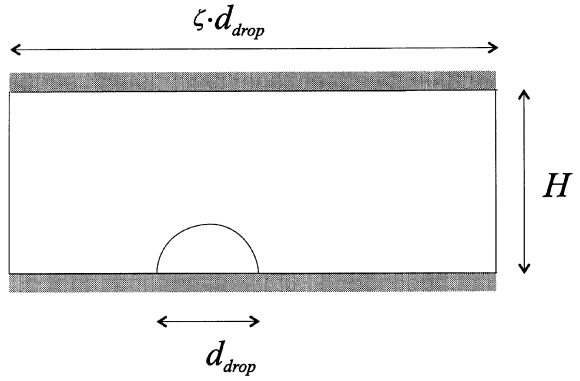

Fig. 11. Schematic of unit cell of gas-sided flow, encompassing one large drop. Definition of ζ.

3.5. Mass transfer from flat parts of plate

It is interesting to compare the Sherwood values for the flat plate parts in between drops, measured with naphthalene, with the ones obtained from measurements without condensation (see Fig. 7) using the analogy of heat and mass transfer. Figure 13 gives this comparison. The naphthalene experiments for a flat plate only, indicated by filled diamonds, are fitted with a dashed line. However, the 2×3 cm^2 pieces of naphthalene are not perfectly flat and have a ca 30 μm edge, see Fig. 4. This explains that these values are higher with respect to the solid line values of the correlation (12). The dotted line in Fig. 13 fits the data of flat parts in between drops, and is in between the two other curves.

It is concluded that mass transfer rates to flat parts in between drops is about as high as the mass transfer rates to flat parts without drops, despite the occurrence of wakes. A quantification of the differences would require experiments more accurate than the ones here presented.

3.6. Interface temperature in dropwise condensation

The correlation (15) for $Sh_{L_{\mathrm{eff}}}$ has been used in the computation method of interface temperatures described in Section 2.4. In the experiments considered, an air–steam mixture with φ_{in} in 20–50% and $Re_{\mathrm{g,in}}$ in 600–1200 was condensed in both compartments of the compact heat exchanger. $Re_{\mathrm{cool}}=430$, $T_{\mathrm{cool}}=25$°C, $T_{\mathrm{g,in}}$ is in 70–80°C. The wetted area ratio has been photographically measured, yielding 0.36 ± 0.03 on the average. For the parameter ζ in equation (14) the value 3 could be used. The average drop diameter has been determined from photographs and video recordings, yielding

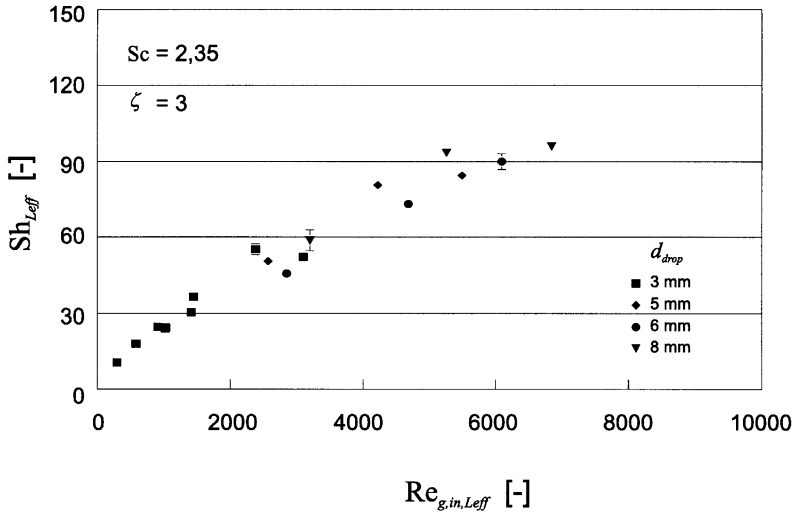

Fig. 12. Sherwood numbers, located on L_{eff}, see equation (14) vs. Reynolds number, based on L_{eff}.

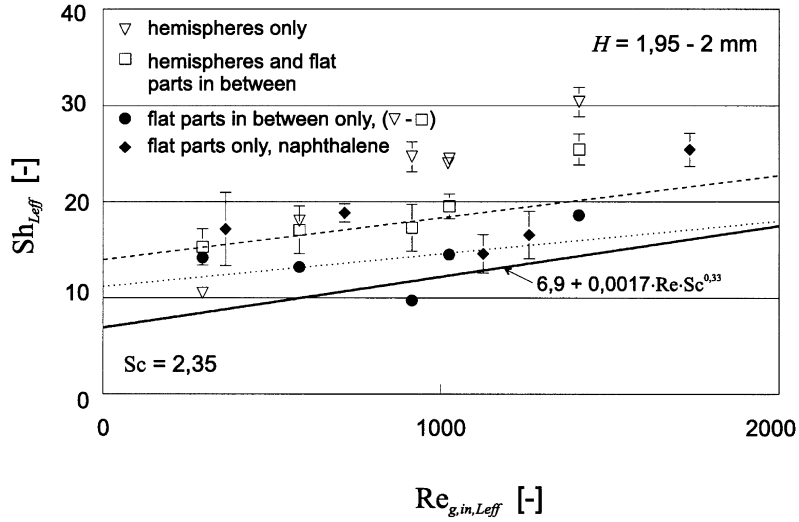

Fig. 13. Comparison of Sherwood numbers measured isothermally for flat parts of the condenser plate.

$d_{\text{drop}} = 0.28 \pm 0.03$ mm, see Ganzevles and van der Geld [9]. The average interface temperature has been measured with an IR-camera, see Section 2.4 and Ganzevles and van der Geld [22].

In Fig. 14 measured and computed temperatures are compared. The error in T_{cond} is 0.2 K, and that of the measured interface temperature is 0.5 K, based on a bandwidth of 10 K of the IR-camera and ca 25 000 (average) drop temperatures (250 per frame) per measuring point indicated in Fig. 14. The agreement is good, showing that the averaged interface temperature can conveniently be estimated using the method of Section 2.4 and the correlation (15) for $Sh_{L_{\text{eff}}}$.

4. Conclusions

The mass transfer from hemispheres on a flat plate to air, flowing internally between two plates, has been measured with the naphthalene sublimation technique. For $Sc = 2.35$ and $Re_{\text{g,in}}$ in 200–9000, $Re_{\text{g,in}} = 2\rho_{\text{g}} \cdot H \cdot u/\eta_{\text{g}}$ based on the distance H of the plates, the

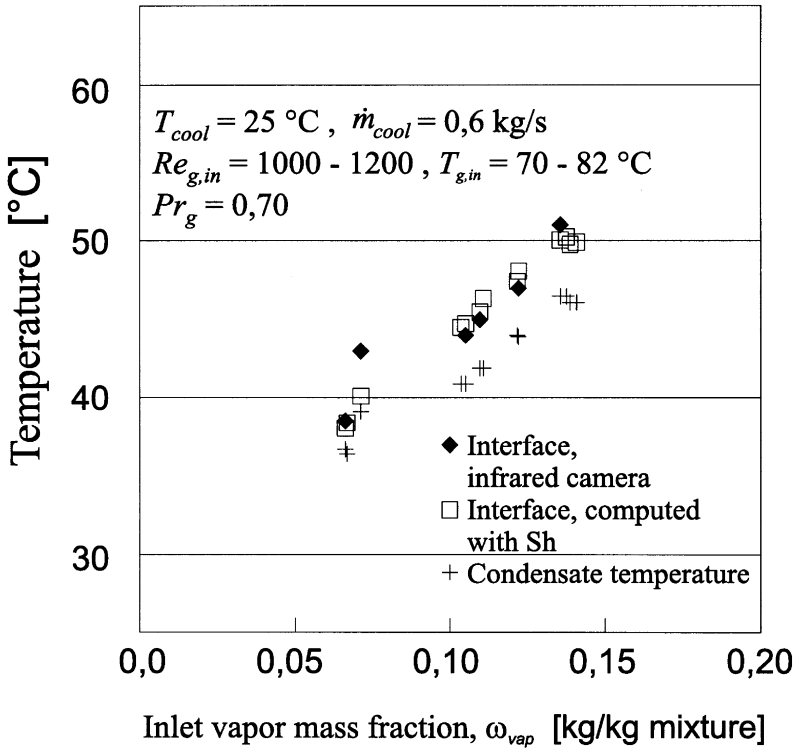

Fig. 14. Comparison of interfacial temperatures measured with infrared camera and computed using the Sherwood number correlation (15).

results for the drop diameter, d_{drop}, equal to 3 mm are correlated as $Sh = a + b \cdot Re_{\text{g,in}} \cdot Sc^{1/3}$, with $a \approx 9$, $b = 0.015 \pm 0.002$ and $Sh = 2h_{\text{m}} \cdot H/\mathbb{D}_{\text{na}}$.

The length scales, H and d_{drop}, are found to be important. A characteristic length scale has been introduced to take both length scales into simultaneous account:

$$L_{\text{eff}} \overset{\text{def}}{=} 2H \Big/ \left(1 + \frac{1}{\zeta} \cdot \frac{H}{d_{\text{drop}}}\right).$$

For $d_{\text{drop}} = 3$–8 mm and $H = 1.95$–6 mm, and both the Sherwood and Reynolds number based on L_{eff} with $\zeta = 3$, the results are correlated for $Re_{\text{g,in},L_{\text{eff}}}$ in 200–6000 as $Sh_{L_{\text{eff}}} = (13 \pm 5) + (0.010 \pm 0.001) \cdot Re_{\text{g,in}} \cdot Sc^{1/3}$. The parameter ζ is the inverse of the wetted area fraction, and therefore represents the drop concentration. As shown by Fig. 12, the use of L_{eff} satisfactorily eliminates the dependency on d_{drop} that the Sherwood number based on D_{H} would show.

In addition, the convective heat transfer from air, flowing internally between two (nearly) flat plates is measured. For $Re_{\text{g,in}}$ in 600–1400, $Re_{\text{g,in}} = 2\rho_{\text{g}} \cdot H \cdot u/\eta_{\text{g}}$ based on the distance between the plates, the heat transfer results are correlated in the form $Nu = a + b \cdot Re_{\text{g,in}} \cdot Pr^{1/3}$ with $a = 6.9 \pm 0.2$ and $b = 0.0017 \pm 0.0002$. Here Nu is also based on $2H$. Using the analogy of heat and mass transfer, these results are compared with the measured mass transfer from the parts of flat plate in between hemispheres. The average mass transfer coefficients have about the same magnitude.

Based on the above findings, the average interfacial temperature has been predicted in actual condensation experiments of water–steam mixtures in a PVDF compact heat exchanger. The calculated temperatures have been verified with an infrared camera. Generally a good agreement is found.

Acknowledgement

The authors are grateful to SHELL Internationale Petroleum Maatschappij B.V. for financial support.

References

[1] von Eucken A. Energie- und Stoffaustausch an Grenzflächen (in German). Die Naturwissenschaften 1937;25:209–18.

[2] Tanner DW, Potter CJ, Pope D, West D. Heat transfer in dropwise condensation—Part I. The effects of heat flux,

steam velocity and non condensable gas concentration. Int J Heat Mass Transfer 1965;8:419–26.
[3] Sparrow EM, Minkowycz WJ, Saddy M. Forced convection condensation in the presence of noncondensables and interfacial resistance. Int J Heat Mass Transfer 1967;10:1829–45.
[4] Tanner DW, Pope P, Potter CJ, West D. Heat transfer in dropwise condensation at low steam pressures in the absence and presence of non-condensable gas. Int J Heat Mass Transfer 1968;11:181–90.
[5] Hu X, Zhang L, Jacobi AM. Surface irregularity effects of droplets and retained condensate on local heat transfer to finned tubes in cross-flow. ASHREA Trans: Research 1994;100:375–81.
[6] Goldstein RJ, Jabbari MY, Chen SB. Convective mass transfer and pressure loss characteristics of staggered short pin-fin arrays. Int J Heat Mass Transfer 1994;37 Suppl 1: 149–69.
[7] Payvar P, Lee YN, Minkowyzc WJ. Simulation of heat transfer to flow in radial grooves of friction pairs. Int J Heat Mass Transfer 1994;37:313–9.
[8] Feron PHM. Hydrodynamics and mass transfer in obstructed narrow channels. Ph.D. thesis, Cranfield University, UK, 1991.
[9] Ganzevles FLA, van der Geld CWM. In situ measurements of wetting rate and local temperatures with dropwise condensation in a compact heat exchanger. Proceedings of the 30th National Heat Conference, HTD-314 vol. 12. New York: ASME, 1995, pp. 68–76.
[10] van der Geld CWM, Brouwers HJH. The mean condensate heat resistance of dropwise condensation with flowing inert gases. Heat and Mass Transfer 1995;30:435–45.
[11] DIN Durchflußmessung mit Blenden, Düsen and Venturirohren in voll durchströmten Rohren mit Kreisquerschnit (in German). Berlin: Beuth Verlag GMBH, 1982.
[12] Reid RC, Prausnitz JM, Poling BE. The Properties of Gases and Liquids. 4th ed. New York: McGraw-Hill, 1987. pp. 208–9.
[13] Ganzevles FLA, van der Geld CWM. The shape of conduction in a multiple channel slab and effect of non-uniform temperatures. Int J Heat Mass Transfer 1997;40:2493–8.
[14] V.D.I.-Wärmeatlas (5. Aufl., in German), pp. Ca2–6 and p. Ca20 (Bild 14). V.D.I. Verlag GmbH, Düsseldorf, 1988.
[15] Shah RK, London AL. Laminar flow forced convection in ducts. Chap. VI and VII. London: Academic Press, 1978.
[16] Bird RB, Steward WE, Lightfoot EN. Transport phenomena. 1st ed. New York: Wiley, 1960. p. 646.
[17] Ambrose D, Lawrenson IJ, Sprake CHS. The vapour pressure of naphthalene. J Chem Thermodynamics 1975;7:1173–6.
[18] Cho K, Irvine TF, Karni J. Measurement of the diffusion coefficient of naphthalene into air. Int J Heat Mass Transfer 1992;35:957–66.
[19] Kline SJ, McClintock FA. Describing uncertainties in single-sample experiments. Mech Eng 1953;75:3–8.
[20] Stephan K. Wärmeübertragung und Druckabfall bei nicht ausgebildeter Laminarströmung in Rohren und in ebenen Spalten (in German), Chemie-Ing Techn 1959;31:773–8.
[21] Fiebig M, Grosse-Gorgemann A, Hahne W, Leiner W, Lorentz S, Mitra NK, Weber D. Local heat transfer and flow structure in grooved channels: measurements and computations. Proceedings of the 10th Int Heat Transfer Conference. 1994;4 8-IC-8:237–41.
[22] Ganzevles FLA, van der Geld CWM. Marangoni convection in binary drops in air cooled from below. Int J Heat Mass Transfer 1998;41:1293–301.